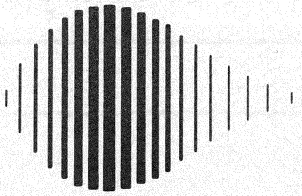

NATIONAL CENTER FOR EARTHQUAKE ENGINEERING RESEARCH

State University of New York at Buffalo

MODELING STRONG GROUND MOTION FROM MULTIPLE EVENT EARTHQUAKES

by

Glenn W. Ellis[1] and Ahmet S. Cakmak[2]

Department of Civil Engineering and Operations Research
School of Engineering and Applied Science
Princeton University
Princeton, New Jersey 08544

Technical Report NCEER-88-0042

October 15, 1988

This research was conducted at Princeton University and was partially supported by the National Science Foundation under Grant No. ECE 86-07591.

NOTICE

This report was prepared by Princeton University as a result of research sponsored by the National Center for Earthquake Engineering Research (NCEER). Neither NCEER, associates of NCEER, its sponsors, Princeton University or any person acting on their behalf:

a. makes any warranty, express or implied, with respect to the use of any information, apparatus, method, or process disclosed in this report or that such use may not infringe upon privately owned rights; or

b. assumes any liabilities of whatsoever kind with respect to the use of, or the damage resulting from the use of, any information, apparatus, method or process disclosed in this report.

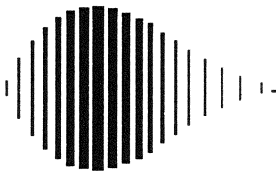

MODELING STRONG GROUND MOTION FROM MULTIPLE EVENT EARTHQUAKES

by

Glenn W. Ellis[1] and Ahmet S. Cakmak[2]

October 15, 1988

Technical Report NCEER-88-0042

NCEER Contract Number 87-3002

NSF Master Contract Number ECE 86-07591

1 Assistant Professor, Dept. of Civil and Environmental Engineering, Clarkson University
2 Professor, Dept. of Civil Engineering and Operations Research, Princeton University

NATIONAL CENTER FOR EARTHQUAKE ENGINEERING RESEARCH
State University of New York at Buffalo
Red Jacket Quadrangle, Buffalo, NY 14261

PREFACE

The National Center for Earthquake Engineering Research (NCEER) is devoted to the expansion and dissemination of knowledge about earthquakes, the improvement of earthquake-resistant design, and the implementation of seismic hazard mitigation procedures to minimize loss of lives and property. The emphasis is on structures and lifelines that are found in zones of moderate to high seismicity throughout the United States.

NCEER's research is being carried out in an integrated and coordinated manner following a structured program. The current research program comprises four main areas:

- Existing and New Structures
- Secondary and Protective Systems
- Lifeline Systems
- Disaster Research and Planning

This technical report pertains to Program 1, Existing and New Structures, and more specifically to geotechnical studies, soils and soil-structure interaction.

The long term goal of research in Existing and New Structures is to develop seismic hazard mitigation procedures through rational probabilistic risk assessment for damage or collapse of structures, mainly existing buildings, in regions of moderate to high seismicity. The work relies on improved definitions of seismicity and site response, experimental and analytical evaluations of systems response, and more accurate assessment of risk factors. This technology will be incorporated in expert systems tools and improved code formats for existing and new structures. Methods of retrofit will also be developed. When this work is completed, it should be possible to characterize and quantify societal impact of seismic risk in various geographical regions and large municipalities. Toward this goal, the program has been divided into five components, as shown in the figure below:

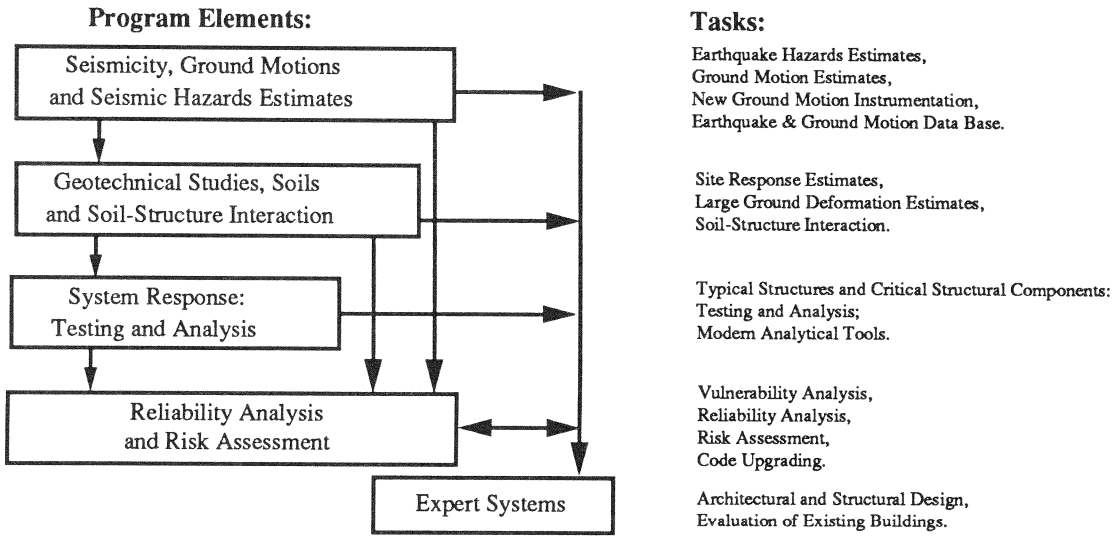

Geotechnical studies, soils and soil-structure interaction constitute one of the important areas of research in Existing and New Structures. Current research activities include the following:

1. Development of linear and nonlinear site response estimates.
2. Development of liquefaction and large ground deformation estimates.
3. Investigation of soil-structure interaction phenomena.
4. Development of computational methods.
5. Incorporation of local soil effects and soil-structure interaction into existing codes.

The ultimate goal of projects in this area is to develop methods of engineering estimation of large soil deformations, site response, and the effects that the interaction of structures and soils have on the resistance of structures against earthquakes.

This study represents work being done in the area of site response analysis. Currently, few sites have actual recordings of strong ground motion, and simple procedures for simulating multiple event earthquakes do not exist. In order to provide accurate, strong ground motion input to structural models which accommodate multiple event earthquakes, the researchers compiled a database of strong motion accelerograms, and modeled them using an ARMA process. The resulting simulations provided realistic duration, frequency content, intensity and number of periods of shaking for the site and source variables. The simulation results can be used to develop seismic hazard curves for a given site.

ABSTRACT

Large earthquakes are often made up of several subevents. Thus the cumulative damage is higher than for single event earthquakes. Many procedures have been developed to simulate earthquake ground motion occurring from a single energy release; however, procedures to model accelerograms with several periods of strong shaking and to relate the modelling parameters to physical variables have not been developed.

In this research, a database of strong motion accelerograms from multiple event earthquakes including the 1978 Miyagiken-Oki Earthquake, the 1968 Tokachi-Oki Earthquake, the 1983 Nihonkai-Chubu Earthquake, and the 1985 Michoacan Earthquake were modelled by an ARMA process after first processing the records with multivariate variance and frequency stabilizing transformations. The modelling parameters were related to the time, magnitude, and location of each subevent and to the site conditions using a regression analysis.

ACKNOWLEDGEMENTS

We would like to thank Dr. M. Miyamura and Mr. K. Kanda of Kobori Research, Kajima Corporation, Japan; Mr. Eiichi Kurata of the Port and Habor Research Institute, Japan; and Mr. Yoshihiro Sawada of the Central Research Institute of the Electric Power Industry, Japan for providing the multiple peak Japanese acceleration data analyzed in this report.

TABLE OF CONTENTS

LIST OF ILLUSTRATIONS

LIST OF ILLUSTRATIONS

LIST OF TABLES

SECTION 1
INTRODUCTION

The damage incurred by structures during an earthquake depends on both the nature of the structure and the properties of the ground motion. However, few sites have recordings of strong ground motion. To provide input motions to structural models for sites for which no strong motion accelerograms exist, it is necessary to simulate the ground motion.

Many procedures exist for simulating ground motion from a single energy release. Models for simulating the frequency spectra of the ground motion are useful in predicting the response of linear structural models, but do not work well to predict nonlinear response. Simulated accelerograms can also be used as input motion. However, simple procedures for simulating accelerograms from multiple shock earthquakes based on historical data do not exist. Depending on the location and time of each subevent, simulations with several periods of strong shaking may be needed. These accelerograms will result in higher cumulative damage to structural models than single event earthquakes. To simulate these records, a modeling procedure which can measure and simulate accelerograms with several sections of strong shaking is needed.

In this report, the results of modeling a large database of strong motion accelerograms from multiple event earthquakes using a procedure based on Ellis et al. (1988) is presented. An overview of this procedure is shown in Fig. 1.1. Because of the use of a standard deviation function to model the intensity of shaking, the procedure can be used to efficiently generate simulations with multiple periods of shaking. By relating the modeling parameters to physical variables through a regression analysis, it is possible to simulate the ground motion of multiple event earthquakes for sites where no strong motion data exists. These simulations will have realistic duration, frequency content, intensity, and number of periods of shaking for the site and source variables. Also, because accelerograms often show different behavior under similar conditions, the variability in ground motion is measured by the standard errors of the regression parameters. This makes it possible to generate many simulations with varying properties within the range of the expected ground motion.

(a) Collect database of multiple event accelerograms

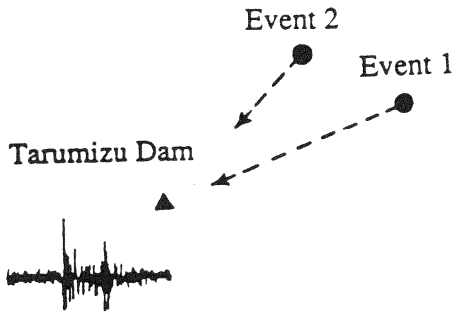

(b) Model accelerograms

-- Variance and frequency stabilizing transformations

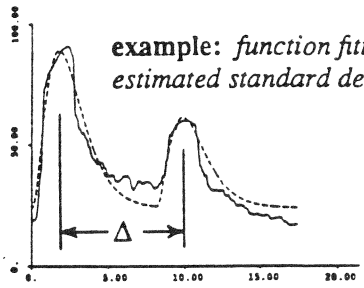

-- Model stabilized series with ARMA process

(c) Relate modelling parameters to physical variables

example: Δ = function of the time and hypocentral distance to each subevent

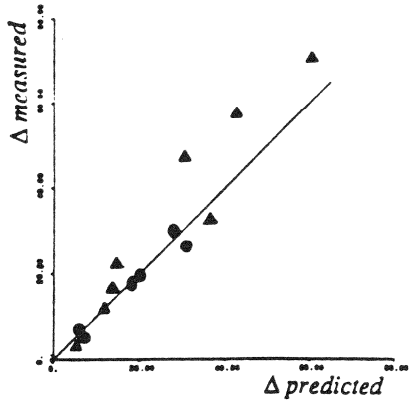

(d) Validation of Modelling Procedure

-- Simulate accelerogram

-- Compare Fourier and response spectra of original and simulated accelerogram

-- Compare response of nonlinear structural models to original and simulated ground motion

Fig. 1.1 Procedure for Modeling Multiple Event Earthquakes.

SECTION 2
MULTIPLE EVENT EARTHQUAKES

Multiple shock earthquakes occur when the rupture reaches a barrier which stops the faulting. Various types of barriers have been proposed by Aki (1978). These can be classified as either geometric discontinuities or inhomogeneities at the plate interface. Geometric discontinuities include bends in the fault or a junction of faults. The inhomogeneities may be either ductile or brittle barriers.

Large earthquakes are often made up of several subevents. This is due to the longer fault length increasing the probability of encountering a barrier. Examples for which strong motion accelerograms have been recorded include the 1978 Miyagiken-Oki Earthquake (M=7.8), the 1968 Tokachi-Oki Earthquake (M=8.0), the 1983 Nihonkai-Chubu Earthquake (M=7.7), and the 1985 Michoacan Earthquake (M=8.1). Figure 2.1 shows accelerograms recorded from three of these earthquakes which occurred in Japan. Each earthquake produced accelerograms with a single period of strong shaking and also accelerograms having two or three periods of strong shaking. Accelerograms with several periods of strong shaking occur when energy from each subevent arrives at separate times. The time of arrival of each subevent i is

$$t_i' = t_i + \frac{d_i}{v_s}, \tag{2.1}$$

where

t_i' = the time of arrival of energy from subevent i,

t_i = the time of the subevent i,

d_i = the hypocentral distance from the recording station to subevent i,

v_s = the shear wave velocity.

Thus the time between sections of strong shaking and the overall duration of strong shaking are functions of the distance between the recording station and each subevent, the time of each subevent, and the soil velocity.

Accelerograms of multiple event earthquakes that have only one period of strong shaking may occur for several reasons. If the recording station is located far from the subevents, the seismic waves go through many random reflections, refractions, and attenuations before reaching the recording site. This results in accelerograms of long

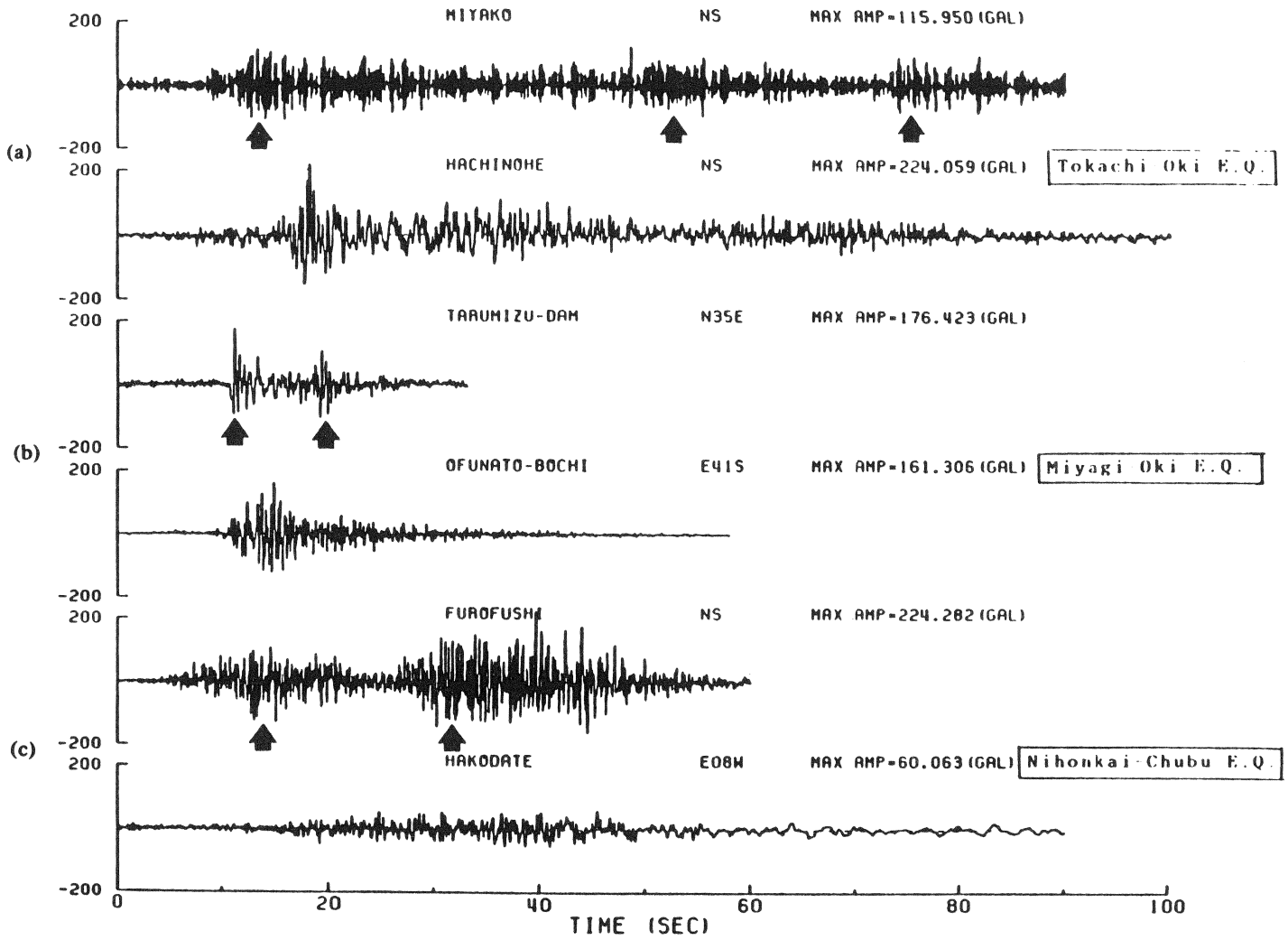

Fig. 2.1 Recorded Ground Motion From the (a) Tokachi-Oki Earthquake, (b) Miyagiken-Oki Earthquake, and (c) Nihonkai-Chubu Earthquake.

duration and uniform intensity. If a recording station is located closer to a second subevent than the first, then the seismic waves from both subevents may arrive at the same time. This results in an accelerogram of short duration and strong intensity.

In the following sections, descriptions of the source characteristics of the four earthquakes used in this study are presented. Each earthquake consisted of either two or three separate shocks.

2.1. 1968 Tokachi-Oki Earthquake

The 1968 Tokachi-Oki Earthquake occurred off the coast of Tokachi, Hokkaido, Japan on May 16, 1968. The faulting mechanism was interpreted as a low-angle thrust fault with a considerable strike-slip component. The oceanic side underthrusted below the continent side (Kanamori, 1971). The magnitude was estimated as $M_s = 8.0$.

According to Mori and Shimazaki (1984), the earthquake originated on the seaward side of the aftershock region (see Fig. 2.2). Thirty-nine seconds later a subevent occurred to the west of the epicenter. Then, twenty-nine seconds after the first subevent, a second subevent occurred to the north. Thus, the earthquake source actually consisted of three strong centers of energy release which ruptured over a time interval of a minute.

2.2. 1978 Miyagiken-Oki Earthquake

The 1978 Miyagiken-Oki Earthquake occurred off the Pacific coast of the Miyagi prefecture, Japan. The damage from the earthquake resulted in the death of 28 persons, 1325 injuries, and the collapse of 1183 houses. The cause of the earthquake has been interpreted as a rebound at the interface between the continental and oceanic lithospheres, resulting in predominantly thrust faulting (Seno et al., 1980). The magnitude of the shock was 7.4.

It was found that a two-segment model explained the observed waveforms. The model by Seno et al. (1980) proposes a second event of equal proportion occurring about 30 km to the west and 11 seconds after the main shock (see Fig. 2.3). It is assumed that the first event was arrested at a homogeneous barrier with high fracture strength which separated the two events.

2.3. 1983 Nihonkai-Chubu Earthquake

The 1983 Nihonkai-Chubu Earthquake occurred in the Japan Sea about 80 km west of the Aomori and Akita prefectures. According to Sato (1985), the earthquake consisted of two main shocks. Sato estimates the location of the second shock to be 44 km NNE of the first shock as shown in Fig. 2.4. The time delay between the shocks is estimated to be 26 seconds.

2.4. 1985 Michoacan Earthquake

The September 19, 1985 Michoacan earthquake occurred along the Pacific coast of Mexico and recorded a magnitude of 8.1 on the Richter Scale. The depth of the earthquake was estimated at approximately 20 to 30 kilometers. Numerous accelerograms were recorded along the coast by the Guerrero array and in Mexico City. The damage was small near the epicenter, but in Mexico City at a distance of more than 350 kilometers the damage was severe. This was due to the amplification of the seismic waves in the soft sediments below the city.

A two-segment model has been proposed to explain the ground motion. Anderson et al. (1986) estimate that the second shock occurred near station La Union, about 24 seconds after the initial shock (see Fig. 2.5). This explains the multiple periods of shaking at Caleta de Campos and La Villita. Stations to the southeast of La Union show only a single period of shaking due to the simultaneous arrival of waves from the two events.

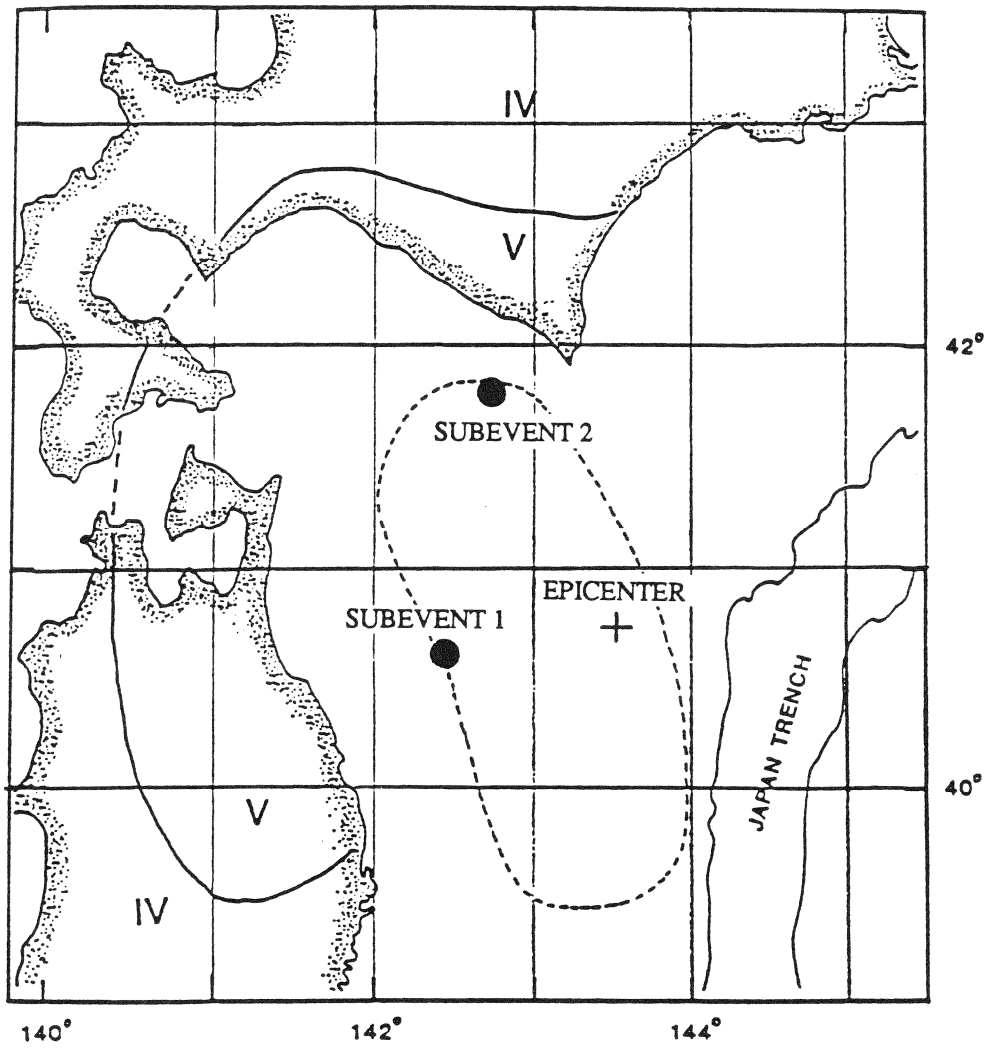

Fig. 2.2 Locations of Energy Release for the 1968 Tokachi-Oki Earthquake (after Mori et al., 1984).

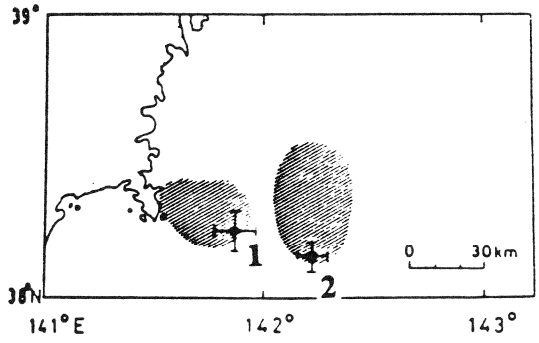

Fig. 2.3 Locations of Energy Release for the 1978 Miyagiken-Oki Earthquake. Standard deviations are indicated by bars and aftershock zones are hatched (after Seno, et al., 1980).

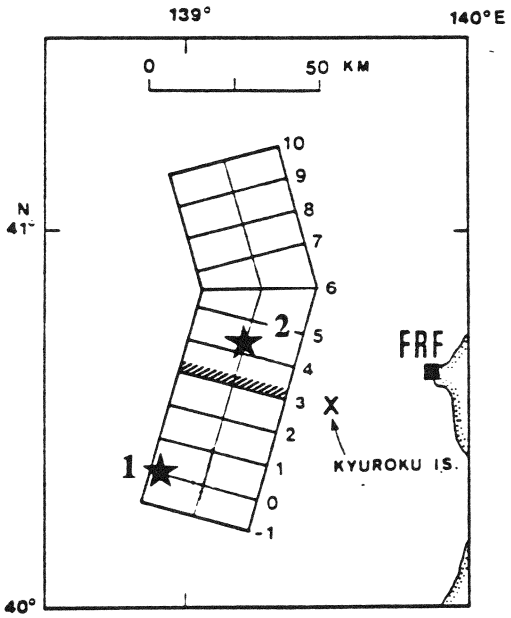

Fig. 2.4 Locations of Energy Release for the 1984 Nihonkai-Chubu Earthquake (after Sato, 1985).

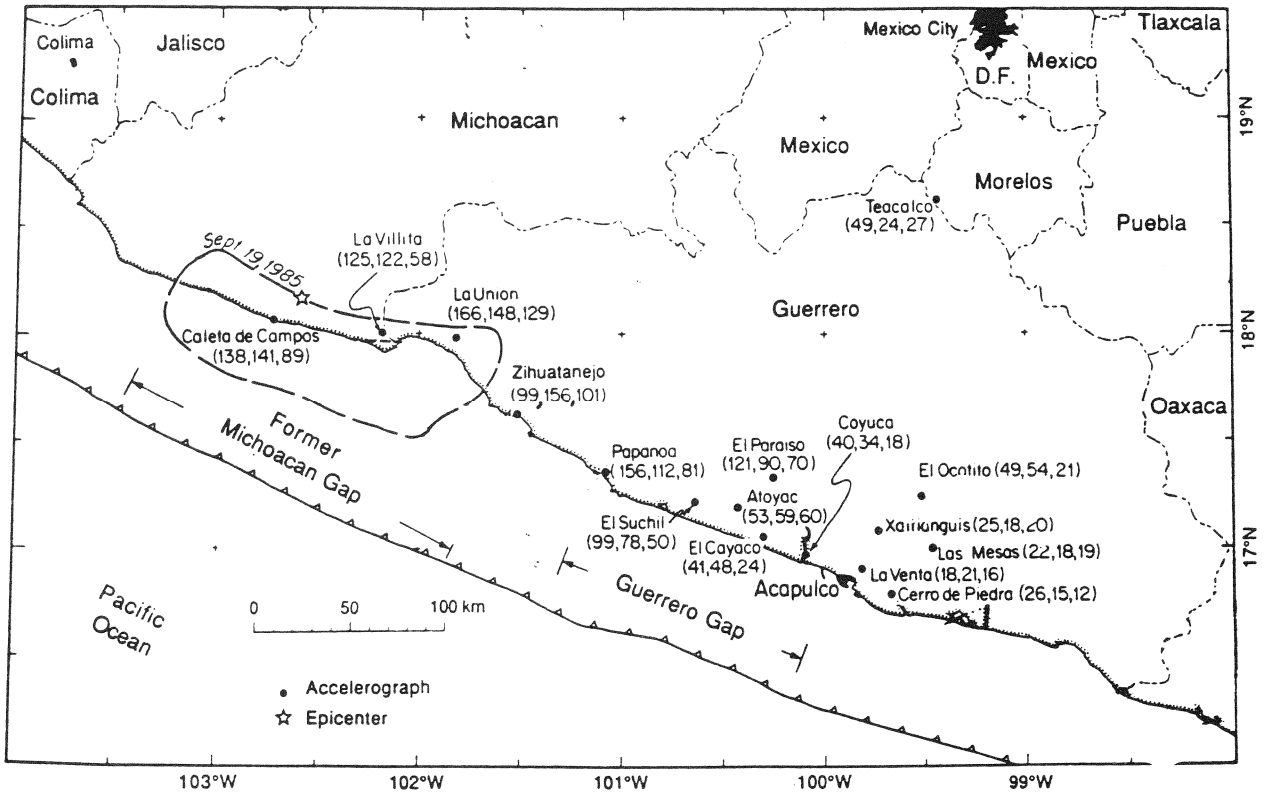

Fig. 2.5 Locations of Epicenter, Stations, and Aftershock Zone for the 1985 Michoacan Earthquake. The second shock occurred near station La Union (after Anderson, et al., 1986).

SECTION 3
MODELING ACCELEROGRAMS WITH ARMA PROCESSES

Many stochastic processes can be approximated by autoregressive-moving average (ARMA) models. In the ARMA model of order (p,q), the current deviation of the process from its mean value μ, $(Z_t - \mu)$, is expressed as a function of previous deviations, a shock a_t, and previous shocks as

(3.1)

$$Z_t - \mu = \phi_1(Z_{t-1} - \mu) + \phi_2(Z_{t-2} - \mu) + \cdots + \phi_p(Z_{t-p} - \mu) + a_t - \theta_1 a_{t-1} - \theta_2 a_{t-2} - \cdots - \theta_q a_{t-q}$$

where

p = order of AR parameters

q = order of MA parameters

ϕ_k = autoregressive parameter at lag k, k=1,2,...,p

θ_k = moving average parameter at lag k, k=1,2,...q

μ = mean level

a_t = white noise sequence with variance, σ_a^2.

The procedures for identifying, fitting, and validating ARMA models are discussed in detail in Box and Jenkins (1976).

Due to the nonstationarity of accelerograms, it is not appropriate to fit an ARMA model directly to the time series. This nonstationarity manifests itself most conspicuously in the large changes of variance over time. However, in most records examined, the frequency content is also variable. Typically, the predominant frequency decreases with time. Three basic approaches have been taken to handle this nonstationarity: (1) fitting time-invariant ARMA parameters to short sections of the original records (Chang et al., 1982), (2) fitting time-varying ARMA parameters to the original records (Kozin, 1977; Jurkevics and Ulrych, 1979; Gersch and Kitagawa, 1985), and (3) fitting time-invariant ARMA parameters to a series stabilized by transformations (Polhemus and Cakmak, 1981; Ellis et al., 1987; Ellis et al., 1988). Because the primary goal of this research is to relate modeling parameters to physical variables

affecting the ground motion, a modeling procedure using single-valued parameters based on the methodology in Polhemus and Cakmak (1981), Ellis et al. (1987) and Ellis et al. (1988) will be used. Before an ARMA process can be fit to the time series, the variance and frequency content of the accelerograms must first be stabilized. ARMA coefficients are then estimated for the stationary series. By analyzing a large number of accelerograms, the parameters generated in the stabilization transformations and the ARMA parameters may then be related to physical variables. Finally, simulations are generated from the modeling parameters to validate the procedure. Details of the stabilization and simulation procedures for accelerograms with single and multiple periods of shaking are discussed in the following sections.

3.1. Variance and Frequency Stabilization - Single Period of Shaking

The original time series are first transformed from Cartesian coordinates (H_1, H_2, and V) into spherical coordinates (ρ, α, and γ).

$$H_1(t) = \rho(t)\cos\gamma(t)\cos a(t) \tag{3.2}$$

$$H_2(t) = \rho(t)\cos\gamma(t)\sin a(t) \tag{3.3}$$

$$V(t) = \rho(t)\sin\gamma(t) \tag{3.4}$$

The vector magnitude, $\rho(t)$, and the vertical angle, $\gamma(t)$, will be used to stabilize the acceleration time series in Cartesian coordinates.

Because accelerograms normally exhibit weak shaking in the beginning and end of the record, they must be shortened to determine the length of the earthquake. After transforming the accelerograms into spherical coordinates, the cumulative energy, I_0, of the accelerograms is calculated from the vector magnitude as

$$I_0 = \sum \rho_i^2 \Delta t \ . \tag{3.5}$$

By dividing the amount of energy of the vector magnitude at any time, t, by the total energy of the vector magnitude, the cumulative energy function is computed. By examining the shape of the cumulative energy function, the duration of the original accelerograms to be modelled is calculated. Typically, the accelerograms in spherical and Cartesian coordinates are shortened by eliminating the beginning of the components corresponding to about 1% energy and the end of the components

corresponding to about 2% energy.

The standard deviation envelope is estimated by squaring the vector magnitude, smoothing it using a running average with a two second time window, and taking the square root. A standard deviation function, $\hat{\sigma}_\rho(t)$, of the form

$$\hat{\sigma}_\rho(t) = c_1(\alpha - k_1)(\frac{t}{\tau})^p e^{-(\frac{c_2}{\tau})t} + k_1 \tag{3.6}$$

where

$$c_1 = \frac{(2\sqrt{3})^p \, e^p}{p^p}$$

$$c_2 = 2\sqrt{3}$$

is then fitted to the standard deviation envelope (see Fig. 3.1b). The parameters of the function are estimated by minimizing the error between the standard deviation envelope and the function to be fit to the envelope using subroutine ZXMIN in the IMSL subroutine library (1977). The value of α is a measure of the maximum of the strong shaking segment. The weak shaking is measured by k_1. The duration of strong shaking is measured by τ, and the product of τ and p measures the time to the maximum of the function, t_{max}.

The vertical angle envelope, $\hat{\gamma}(t)$, is calculated by smoothing the absolute value of the vertical angle. An exponential decay function is then fitted to the vertical angle envelope (see Fig. 3.1a).

$$\hat{\gamma}(t) = (c_3 - \gamma_f)(1 + \frac{t}{b_3})e^{-\frac{t}{b_3}} + \gamma_f \tag{3.7}$$

where c_3 is the initial value of the function, b_3 is the rate of decay, and γ_f is the lower limit of the function. The value of c_3 is estimated as the mean value of $\bar{\gamma}(t)$ during the first 10% of the record. The lower limit of the function, γ_f, is estimated as the mean value of $\bar{\gamma}(t)$ during the final 1/3 of the record. Finally, the value of b_3 is estimated so that the areas under $\hat{\gamma}(t)$ and $\bar{\gamma}(t)$ are equal.

The variance of the time series is stabilized by dividing the accelerogram components by a function of the standard deviation and vertical envelope functions.

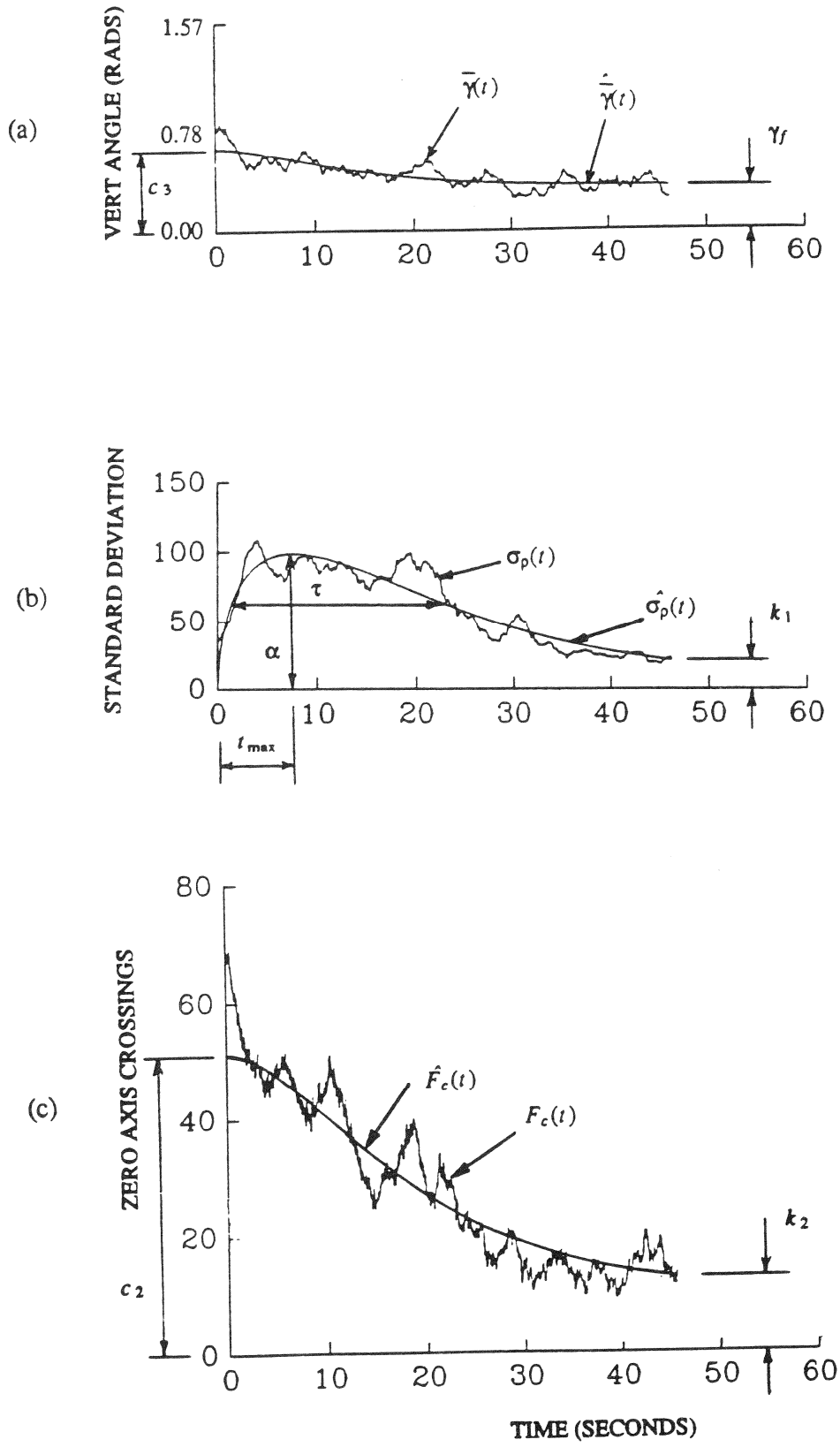

Fig. 3.1 Functions Used to Stabilize the Accelerograms: (a) vertical angle envelope, (b) standard deviation envelope, and (c) frequency envelope.

$$\hat{V}(t) = \frac{V(t)}{\sigma_\rho(t)\,\sin\bar{\gamma}(t)} \tag{3.8}$$

$$\hat{H}_1(t) = \frac{H_1(t)}{\frac{1}{\sqrt{2}}\sigma_\rho(t)\cos\bar{\gamma}(t)} \tag{3.9}$$

$$\hat{H}_2(t) = \frac{H_2(t)}{\frac{1}{\sqrt{2}}\sigma_\rho(t)\cos\bar{\gamma}(t)} \tag{3.10}$$

where H_1, H_2, and V are the original accelerograms and $\hat{H}_1$, $\hat{H}_2$, and $\hat{V}$ are the variance stabilized accelerograms.

Because the frequency content often changes over the length of the record, a frequency stabilizing transformation must also be performed. This is done by using a frequency envelope to change the time scale of the record. The frequency envelope is computed by calculating the crosses per second of each component of the accelerogram, adding them together to get the total number of crosses, and then fitting a smooth function to the total number of crosses. In Fig. 3.1c, the frequency stabilizing function is shown. The same functional form that was used to model the vertical angle envelope is fit to the zero axis crossings.

$$\hat{F}_c(t) = (c_2 - k_2)(1 + \frac{t}{b_2})e^{-\frac{t}{b_2}} + k_2 \tag{3.11}$$

The time increment of the variance stabilized series is changed by multiplying it by a function $\hat{F}_c(t)$ fit to the zero axis crossings.

$$\Delta t' = (\Delta t)\hat{F}_c(t) \tag{3.12}$$

The value of $\Delta t'$ is the new time increment and Δt is the original time increment of 0.02 seconds. The transformed records are then reduced to the same length of time as the initial records and redigitized by linear interpolation. Physically, this expands the time increment in the beginning of the record, where the higher frequencies occur, and decreases the time increment at the end of the record, which is usually dominated by lower frequencies.

3.2. Variance and Frequency Stabilization - Multiple Periods of Shaking

To model accelerograms with more than one segment of strong shaking, only the standard deviation function is modified as shown in Fig. 3.3. For the Miyagiken-Oki

Earthquake recorded at Tarumizu Dam, the second peak occurs about 10 seconds after the first peak due to the different arrival times of the waves from each subevent. To model the standard deviation envelope of a multiple peak event, a function with several peaks is fit to the data.

$$\hat{\sigma}_p(t) = c_1(\alpha_1 - k_1)(\frac{t}{\tau_1})^p e^{-(\frac{c_2}{\tau_1})t} + c_1\alpha_2'(\frac{t-\Delta'}{\tau_2})^p e^{-(\frac{c_2}{\tau_2})(t-\Delta')} + k_1 \qquad (3.13)$$

This function is a summation of the function in Eq. (3.6) with a second function of maximum intensity α_2' with a time lag of Δ'. To relate the modeling parameters to physical variables, the time lag between the peaks of the two periods of strong shaking, Δ, is used. The maximum of each period of strong shaking is measured by α_1 and α_2 respectively. The weak shaking is measured by k_1. The duration of each period of strong shaking is measured by τ_1 and τ_2 respectively. Finally, the parameter p, which describes the shape of the envelopes, is estimated.

3.3. Estimating ARMA Coefficients

In Ellis et al. (1988), it was found that a constrained ARMA (3,1) process fit the data well. The present value of the stabilized time series is a function of past values of the time series and a white noise shock to the system as

$$Z_t - \phi_1 Z_{t-1} - \phi_2 Z_{t-2} - \phi_3 Z_{t-3} = a_t - \theta_1 a_{t-1} \qquad (3.14)$$

where θ_1 is constrained to 0.99. From these parameters, the Fourier spectrum of the fitted model may be calculated. Examples of the Fourier spectra for three Japanese accelerograms are shown in Fig. 3.2. To relate the ARMA parameters to physical variables the three sets of auto-regressive coefficients were factored into a multiplicative model. If the original model is expressed using the backshift operator, B, as

$$(1 - \phi_1 B - \phi_2 B^2 - \phi_3 B^3)Z_t = (1 - \theta_1 B)a_t \qquad (3.15)$$

where B operates such that $BZ_t = Z_{t-1}$, $B^2 Z_t = Z_{t-2}$, etc., then the left hand side of the equation can be factored into an AR(1) and an AR(2) term as

$$(1 - \phi_3' B)(1 - \phi_1' B - \phi_2' B^2)Z_t = (1 - \theta_1 B)a_t \qquad (3.16)$$

where

$$\phi_3' = \frac{1}{r_1}$$

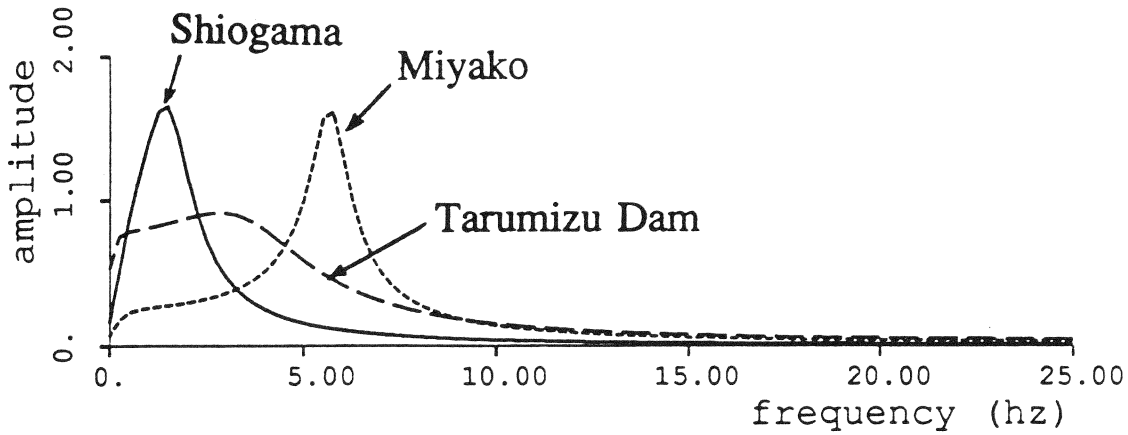

Fig. 3.2 Fourier Spectrum of ARMA Model Fitted to Three Accelerograms Recording the Miyagiken-Oki Earthquake.

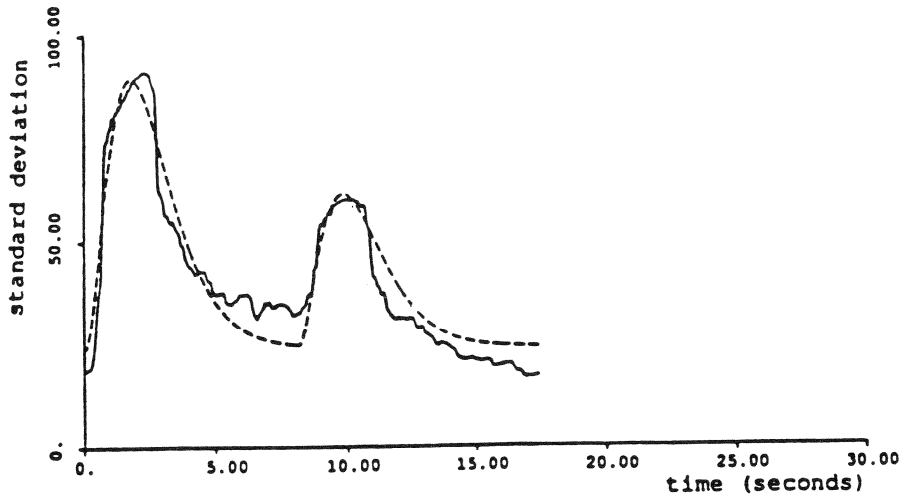

Fig. 3.3 Standard Deviation Function with Multiple Peaks Fitted to an Accelerogram Recorded at Tarumizu Dam.

$$f_2' = -\frac{\phi_3}{\phi_3'}$$

$$\phi_1' = \phi_1 - \phi_3'$$

r_1 = the only real root for B of $1 - \phi_1 B - \phi_2 B^2 - \phi_3 B^3$.

For the multiplicative model shown in Eq. (3.16), the maximum of the Fourier spectrum occurs at the peak of the AR(2) factor. The frequency of the maximum Fourier amplitude of an AR(2) model can be calculated as

$$f_{max} = \frac{50}{2}\pi\cos^{-1}\left[\frac{|\phi_1'|}{2\sqrt{-\phi_2'}}\right]. \tag{3.17}$$

The maximum of the Fourier spectrum can then be calculated by substituting f_{max} computed in Eq. (3.17) into the equation of the Fourier spectrum of an ARMA (3,1) model.

(3.18)

$$F(f) = \left[\frac{2\sigma_a^2(1 + \theta_1^2 - 2\theta_1\cos 2\pi\frac{f}{50})}{[50(2\pi)][1 + \phi_1'^2 + \phi_2'^2 - 2\phi_1'(1 - \phi_2')\cos 2\pi\frac{f}{50} - 2\phi_2'\cos 4\pi\frac{f}{50}][1 + \phi_3'^2 - 2\phi_3'\cos 2\pi\frac{f}{50}]}\right]^{1/2}$$

Also it was found that the summation of the auto-regressive terms was slightly less than one for all of the time series examined.

$$\phi_1 + \phi_2 + \phi_3 \approx 0.99 \tag{3.19}$$

This can be expressed for the multiplicative model as

$$(\phi_1' + \phi_3') + (\phi_2' - \phi_1'\phi_3') - (\phi_2'\phi_3') \approx 0.99\,. \tag{3.20}$$

The exact value of the summation varied for each region studied. Thus the ARMA parameters estimated for each of the series, ϕ_1, ϕ_2, and ϕ_3, were transformed into ARMA parameters representing an equivalent multiplicative model, ϕ_1', ϕ_2', and ϕ_3'. From the multiplicative parameters, the maximum Fourier amplitude, $F(f_{max})$, and the frequency at which the maximum occurs, f_{max}, are calculated. The relationship among the AR parameters in Eq. (3.19) or Eq. (3.20) completes the specification of the model.

3.4. Generating Simulations - Single Period of Shaking

To generate simulations, the modeling procedure is reversed. Given f_{max} and $F(f_{max})$ and Eq. (3.20) the parameters for the multiplicative ARMA model may be calculated by solving Eqs. (3.17), (3.18) and (3.20) for ϕ_1', ϕ_2', and ϕ_3'. From the multiplicative ARMA parameters, the standard ARMA parameters may be calculated by

$$\phi_1 = \phi_1' + \phi_3' \tag{3.21}$$

$$\phi_2 = \phi_2' - \phi_1'\phi_3' \tag{3.22}$$

$$\phi_3 = -\phi_2'\phi_3' . \tag{3.23}$$

From these parameters, three series with stable variance and frequency content are generated by

$$Z_t = \phi_1 Z_{t-1} + \phi_2 Z_{t-2} + \phi_3 Z_{t-3} - \theta_1 a_{t-1} + a_t . \tag{3.24}$$

To introduce the nonstationary frequency content to the series, a zero crossing frequency envelope, $\hat{F}_c(t)$, is computed from Eq. (3.11). Because only the shape and not the magnitude of the frequency envelope is important in rescaling the time scale, the ratio $r_2 = \frac{c_2}{k_2}$ and the rate of decay, b_2, were related to physical variables. Thus to calculate the frequency envelope in Eq. (3.11), the value of k_2 can be chosen as 1.0 and the value of c_2 as r_2. The time axis of each component is rescaled by

$$\Delta t'_s = \frac{0.02}{\hat{F}_c(t)} . \tag{3.25}$$

After changing the time scale of each component, the records are reduced to their original duration by

$$\Delta t''_s = \Delta t'_s \times \frac{\textit{duration of the original simulation}}{\textit{duration of the transformed simulation}} . \tag{3.26}$$

The three components are then digitized into equal increments of 0.02 seconds.

To introduce the nonstationary variance into the simulations, the standard deviation envelope and vertical angle envelope are calculated from Eqs. (3.6) and (3.7). The standard deviation envelopes for the vertical and horizontal components may be calculated by

$$\sigma_v(t) = \sigma_\rho(t)\sin\hat{\gamma}(t) \tag{3.27}$$

$$\sigma_h(t) = \frac{1}{\sqrt{2}}\sigma_\rho(t)\cos\hat{\gamma}(t)\,. \tag{3.28}$$

By multiplying the vertical component by $\sigma_v(t)$ and the two horizontal components by $\sigma_h(t)$, a set of simulations nonstationary in both variance and frequency content is created.

3.5. Generating Simulations - Multiple Periods of Shaking

Simulations with multiple periods of shaking are generated by the method presented in Section 3.4. The only difference is that Eq. (3.13) is used instead of Eq. (3.6) for generating the standard deviation function. In Eq. (3.13), the time lag to the beginning of the second function, Δ', and the height of the second function above the first, α_2', are needed. The parameters which are related to physical variables are the total height of the function at the second peak, α_2, and the time lag between peaks, Δ. The relationship between the parameters Δ' and α_2' and the parameters α_2 and Δ can be calculated by setting the derivative of Eq. (3.13) equal to zero, which will yield the time of the second peak,

$$\frac{d\hat{\sigma}_\rho}{dt} = 0 \tag{3.29}$$

and by setting the value of the function at the second peak equal to α_2,

$$\hat{\sigma}_\rho\left[\frac{p\tau_1}{2\sqrt{3}} + \Delta\right] = \alpha_2. \tag{3.30}$$

In Fig. 3.4, the original accelerogram recorded at Tarumizu Dam from the Miyagiken-Oki Earthquake is compared with a simulation generated by the ARMA modeling procedure. A comparison of the time histories shows similar intensity and duration. Also, the multiple peaks are accurately modelled. In Fig. 3.5, the response spectra and Fourier spectra of the original accelerogram and the simulation are shown. The simulated accelerograms accurately model the shape of the original records.

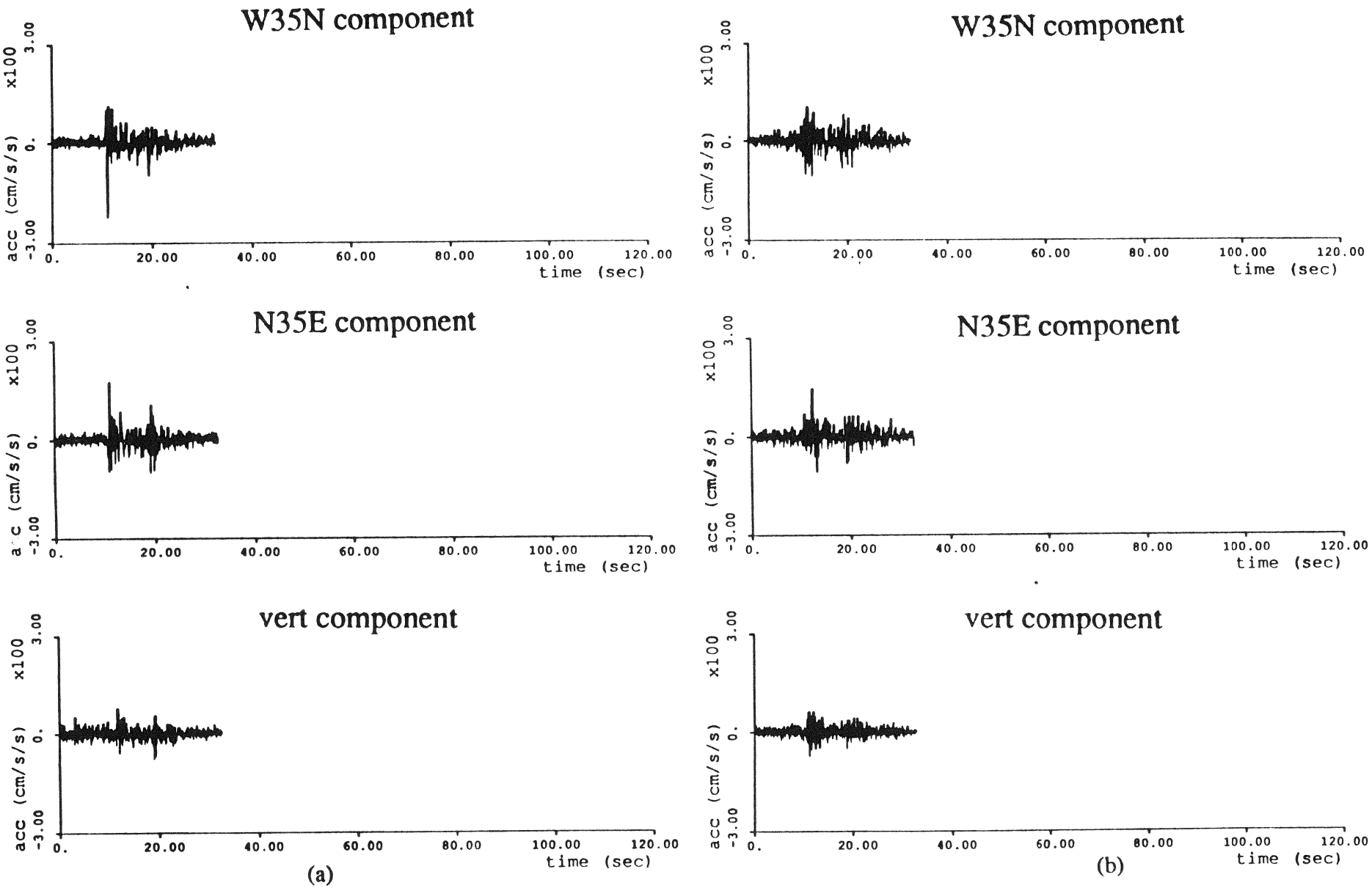

Fig. 3.4 Comparison of (a) Recorded and (b) Simulated Ground Motion at Tarumizu Dam.

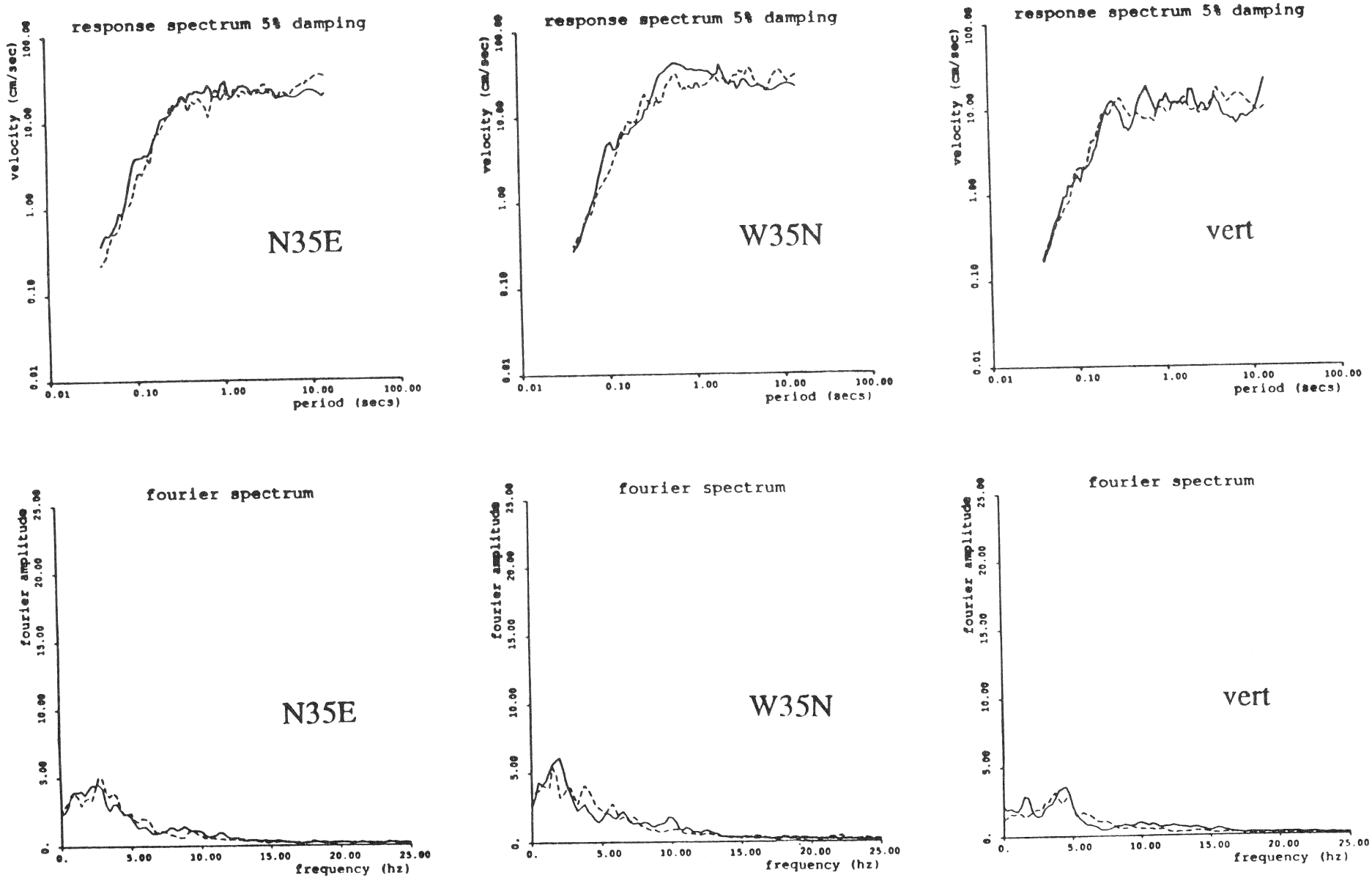

Fig. 3.5 Comparison of Recorded (solid lines) and Simulated (dashed lines) Frequency Spectra for Tarumizu Dam.

SECTION 4
PARAMETRIC RELATIONSHIPS BETWEEN MODELING PARAMETERS AND PHYSICAL VARIABLES

Using the procedure presented in Section 3 for modeling accelerograms with both single and multiple periods of strong shaking, all of the possible ground motion of multiple event earthquakes can be modelled. By analyzing a large number of accelerograms from multiple event earthquakes, relationships between the modeling parameters and physical variables can be found. Through these functional relationships it is possible to produce simulations based on historical data for sites where little or no data exists.

4.1. Relating modeling Parameters to Physical Variables

A database of digitized free-field, strong motion accelerograms recorded from multiple event earthquakes was collected. The Japanese data are referenced in the Port and Habour Research Institute (1968, 1979 and 1983), the Public Works Research Institute, and Sawada et al. The database consists of records from the four earthquakes described in Chapter 2. After the database was assembled, the accelerograms were modelled using the ARMA modeling procedure.

To identify the number of periods of strong shaking, the standard deviation envelope of each accelerogram was calculated. Standard deviation envelopes for the Miyagiken-Oki, Tokachi-Oki, and Nihonkai-Chubu earthquakes are shown in Figs. 4.1, 4.2, and 4.3. As expected, the accelerograms recorded at stations far from the source have a long duration of shaking and a low, broad peak. Records located near the second subevent have a single narrow peak since the energy from both subevents arrives at the recording station at about the same time. At recording stations located near the first subevent, the energy arrives at separate times, resulting in several peaks in the standard deviation envelope. These trends are quantified by relating the parameters of the standard deviation function in Eq. (3.13) to the physical variables of the rupture. For example, the time lag between peaks of the function, Δ, can be related to the hypocentral distance to each subevent and the time of each subevent. The time of arrival of shear waves from each subevent is calculated from Eq. (2.1). The difference between the arrival times is calculated as

$$\Delta = t_2' - t_1'. \tag{4.1}$$

The values of Δ measured from the modeling procedure are compared with the

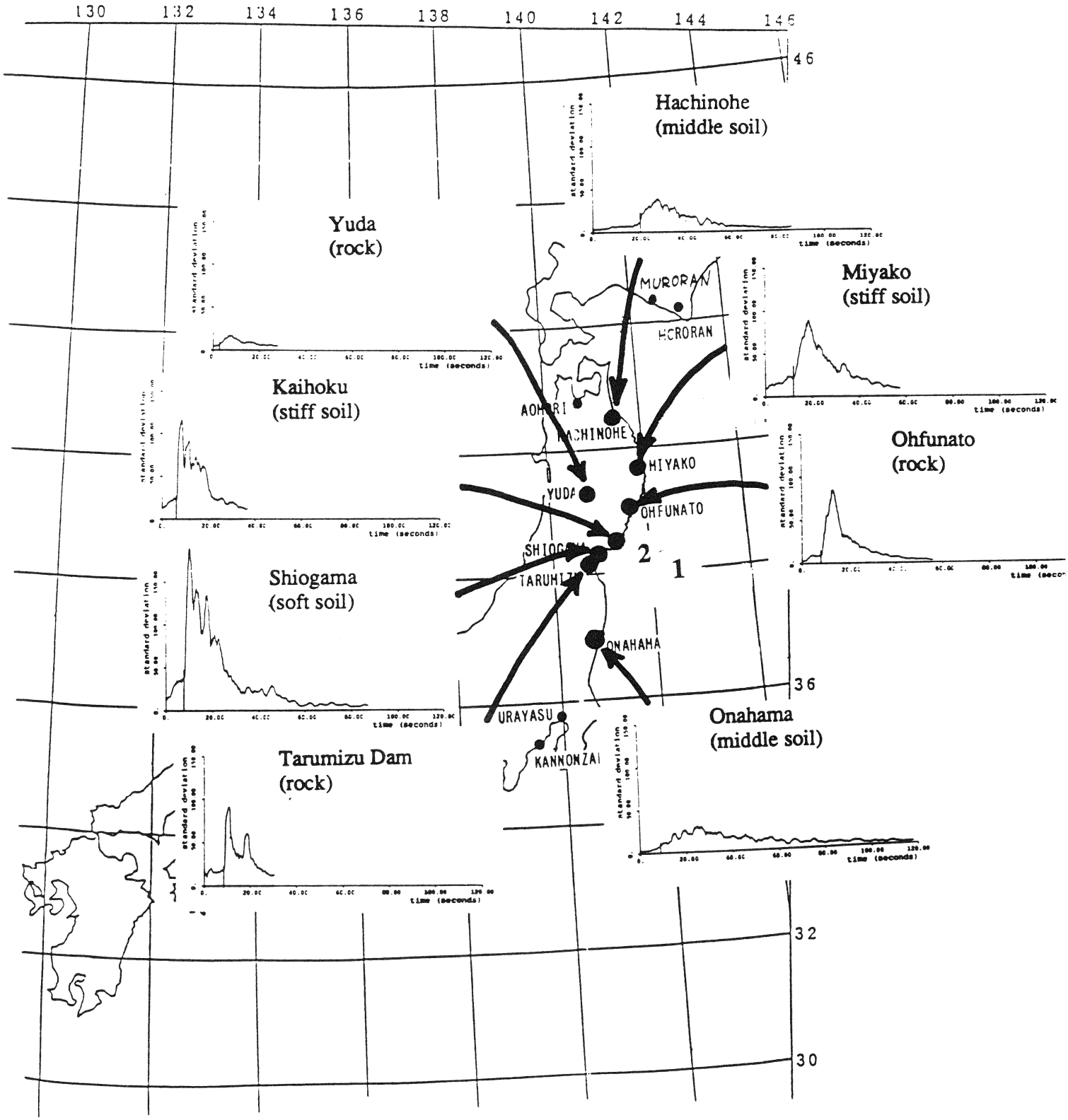

Fig. 4.1 Standard Deviation Envelopes for Sites Recording the Miyagiken-Oki Earthquake.

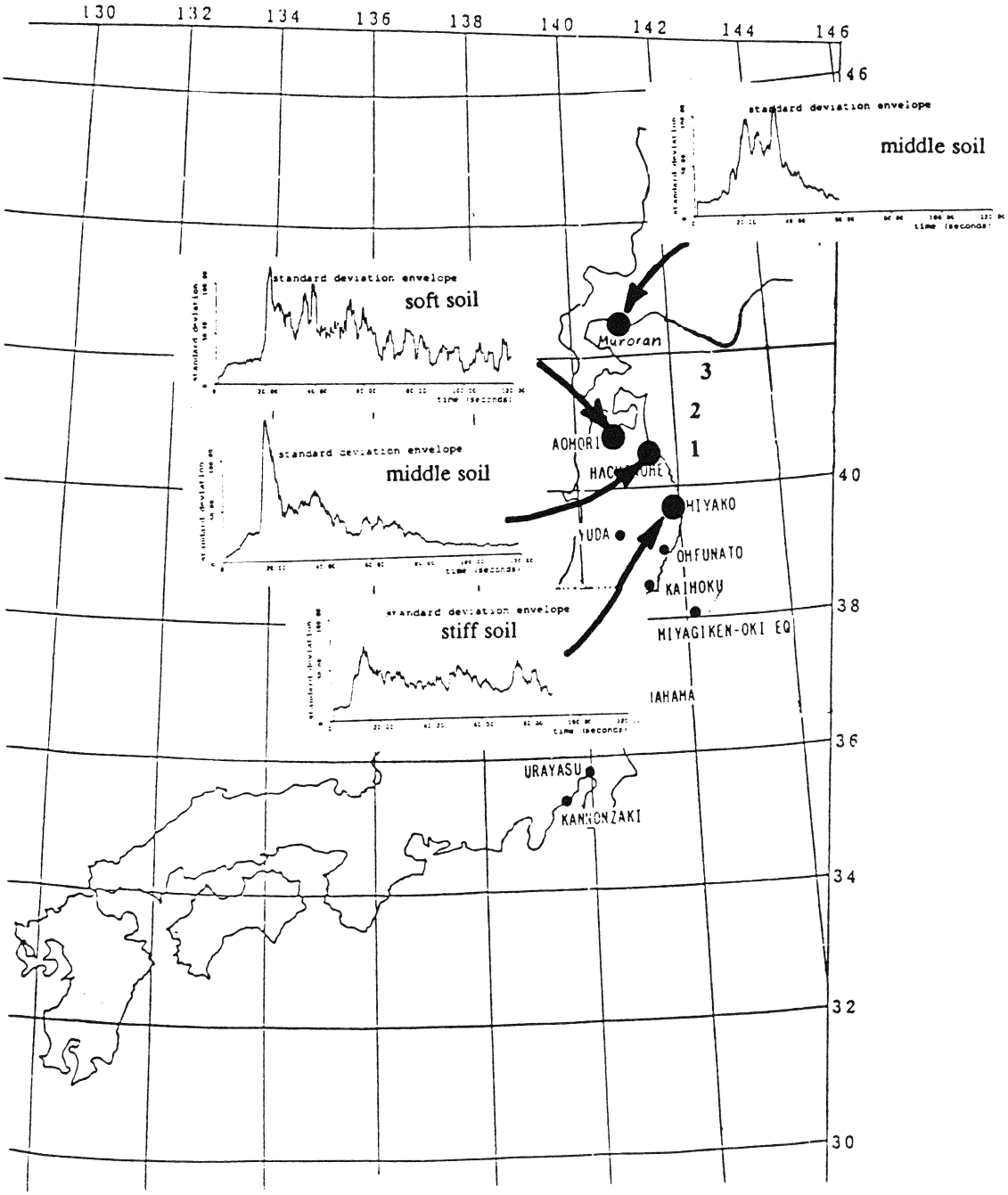

Fig. 4.2 Standard Deviation Envelopes for Sites Recording the Tokachi-Oki Earthquake.

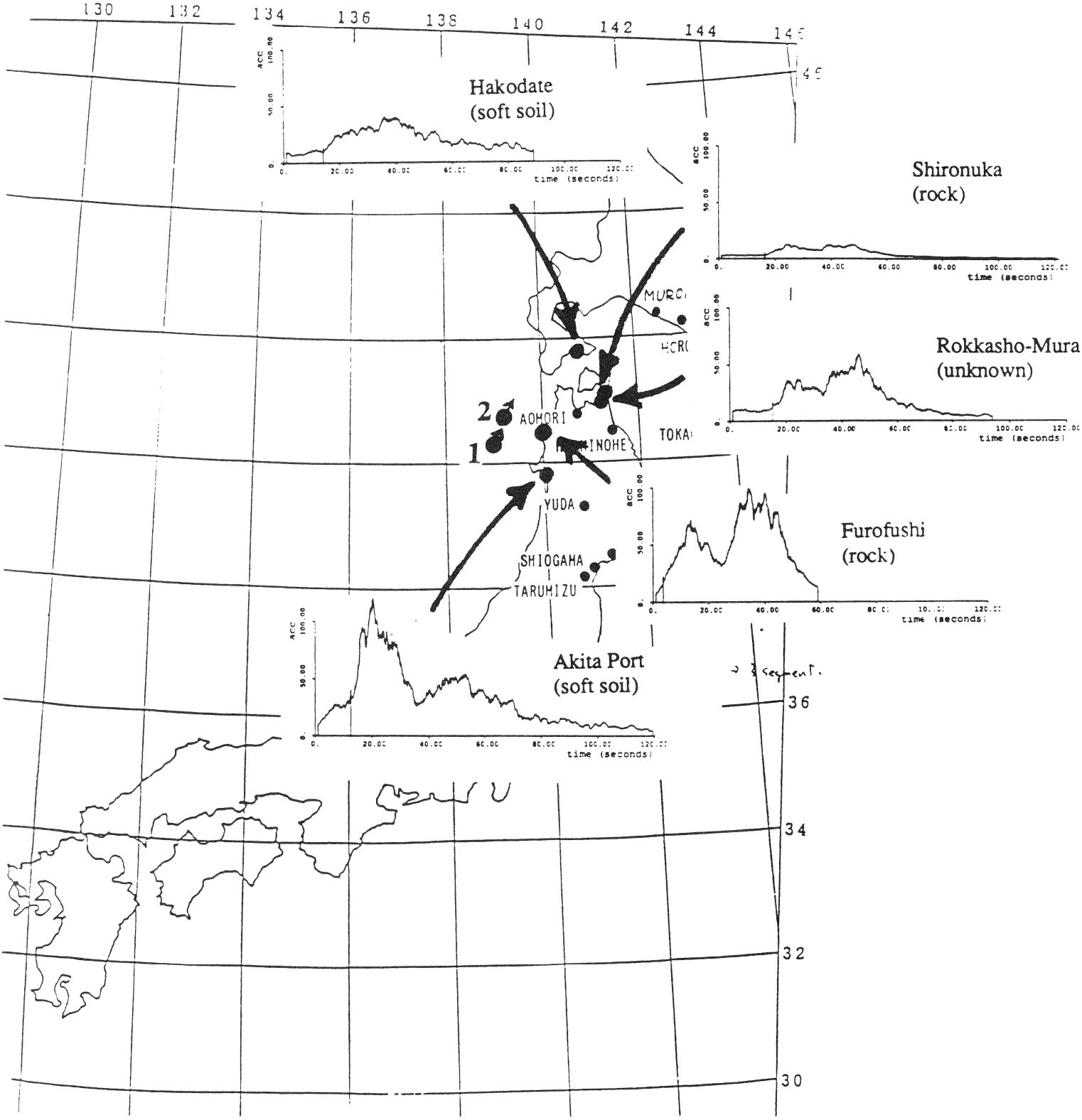

Fig. 4.3 Standard Deviation Envelopes for Sites Recording the Nihonkai-Chubu Earthquake.

values predicted in Eq. (4.1) for the four earthquakes analyzed in Fig. 4.4. The measured and predicted values are in good agreement with r^2 equal to 0.78.

Another important parameter is the maximum of the standard deviation envelope, α. In previous studies for single peak accelerograms (Ellis et al., 1988), α was related to distance, magnitude, and soil type. For multiple peak accelerograms, several α values are measured. To relate these values to physical variables, each subevent is treated separately. Thus α_1 is related to the distance to subevent one, the estimated magnitude of subevent one, and the soil type at the recording station. A similar study was done for each modeling parameter. The results were then compared to previous studies of accelerograms with a single period of strong shaking recorded in Mexico. In Table 4.1, the same functional form for relating modeling parameters and the physical variables for mutiple event and single event earthquakes was used. The estimated coefficients are usually in good agreement considering the standard errors of the estimated values.

4.2. Generating Simulations from Physical Variables

Given the distance to each subevent, the magnitude of each subevent, and the soil type at the recording station, the modeling parameters may be calculated from the parametric relationships shown in Table 4.1, From the modeling parameters, simulations may be generated using the procedure given in Section 3. However, given the physical variables it must first be decided if the accelerogram will have single or multiple periods of shaking.

In Figure 4.5, the occurrence of multiple peak or single peak accelerograms is shown as a function of the predicted time lag between peaks calculated from Eq. (4.1) and the average hypocentral distance. As expected, multiple peaks occur when the predicted time lag between peaks is high. When the predicted time lag is small, the multiple peaks are merged together. Due to the many random reflections and refractions of seismic waves, it is expected that the occurrence of multiple peaks will also be a function of distance. As the distance becomes greater, a larger predicted time lag should be necessary to observe multiple peaks. The data is not sufficient to show this effect.

To generate simulations, the predicted time lag between peaks and the average hypocentral distance are calculated from the given physical variables. From Fig. 4.5, the occurrence of multiple accelerogram peaks may be predicted.

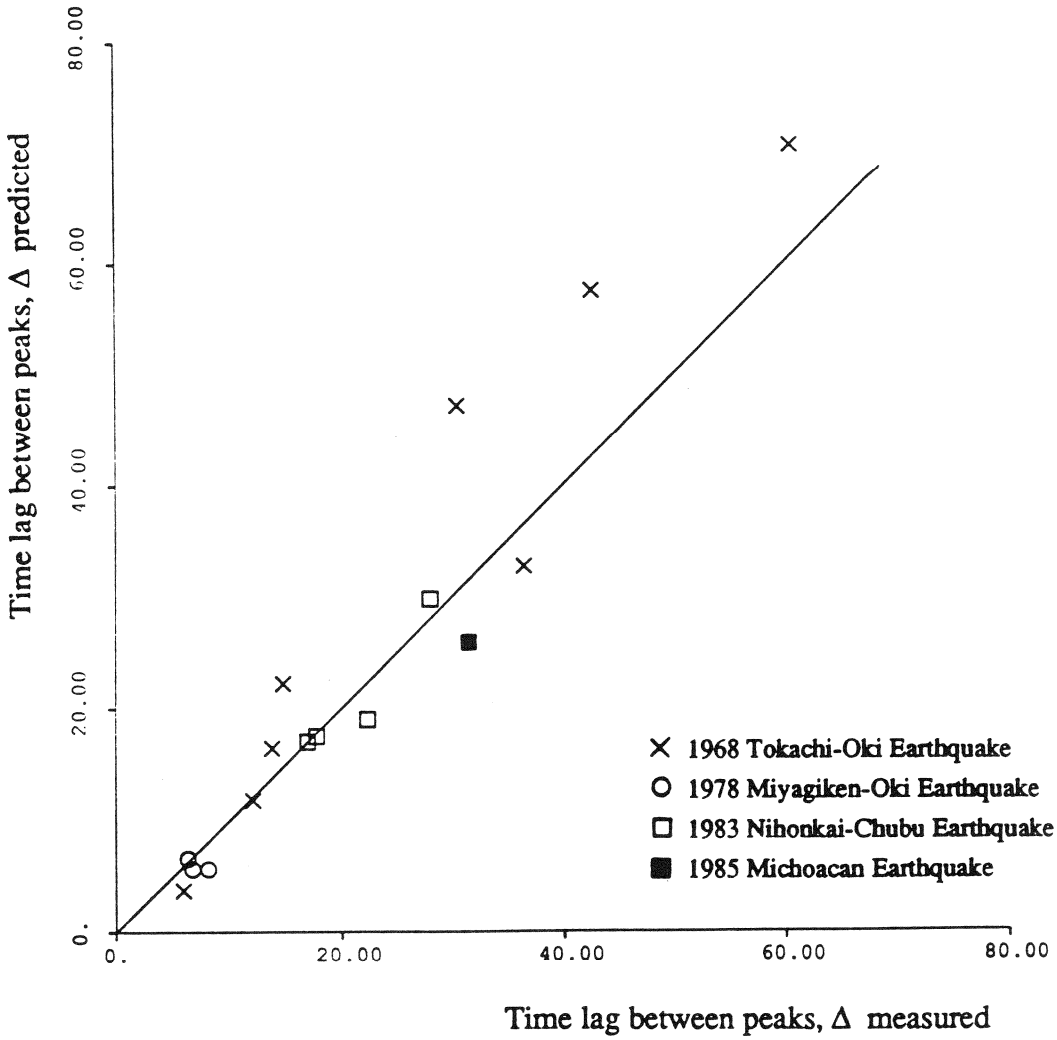

Fig. 4.4 Relationship Between Time Lag Δ Measured from the Accelerograms and the Value of Δ Predicted from Source and Site Locations.

Table 4.1 Comparison of Regression Coefficients Estimated for Single Event and Multiple Event Earthquakes.

d = epicentral distance (km) M = magnitude

SINGLE EVENT	MULTIPLE EVENT
$\alpha = (-1.3\pm13.1) + (13.24\pm2.22)\ln(\frac{10^M}{d^3\gamma_f^3})$	$\alpha = (11.2\pm19.6) + (10.6\pm3.6)\ln(\frac{10^M}{d^3\gamma_f^3})$
$\ln(\tau) = (0.512\pm0.75) + (0.392\pm0.11)M - (3.63\pm1.17)\gamma_f$	$\ln(\tau) = (3.48\pm4.3) - (.16\pm.60)M - (0.33\pm1.42)\gamma_f$
$k_1 = (2.04\pm2.0) + (0.247\pm0.023)\alpha$	$k_1 = (8.66\pm4.45) + (0.134\pm0.066)\alpha$
$\ln(t_{max}) = (1.249\pm0.22) + (0.00377\pm0.00086)d$	$\ln(t_{max}) = (1.3\pm0.33) + (0.0022\pm0.0021)d$
$r_2 = 1.16\pm0.37$	$r_2 = 1.48\pm0.82$
$b_2 = 3.29\pm6.76$	$b_2 = 6.21\pm5.88$
$r_3 = 1.60\pm1.48$	$r_3 = 1.12\pm0.27$
$b_3 = 5.43\pm12.6$	$b_3 = 1.17\pm0.38$
$\gamma_f = f$ (soil type)	$\gamma_f = f$ (soil type)
$\ln(f_{max}) = (2.31\pm0.51) + (3.14\pm0.58)\gamma_f - (0.321\pm0.09)M - (0.00262\pm0.0027)d$	$\ln(f_{max}) = (5.27\pm0.51) + (0.27\pm0.58)\gamma_f - (0.95\pm8.00)M - (0.0018\pm0.0021)d$
$\ln[F(f_{max})] = (-1.08\pm0.11) - (0.0031\pm0.00023)d - (2.25\pm0.29)\gamma_f$	$\ln[F(f_{max})] = (-1.57\pm0.26) - (0.0017\pm0.00093)d - (0.54\pm0.51)\gamma_f$
$\phi_1 + \phi_2 + \phi_3 = (1.010\pm0.0081) - (0.0159\pm0.0019)f_{max}$	$\phi_1 + \phi_2 + \phi_3 = (1.001\pm0.0020) - (0.0020\pm0.0047)f_{max}$

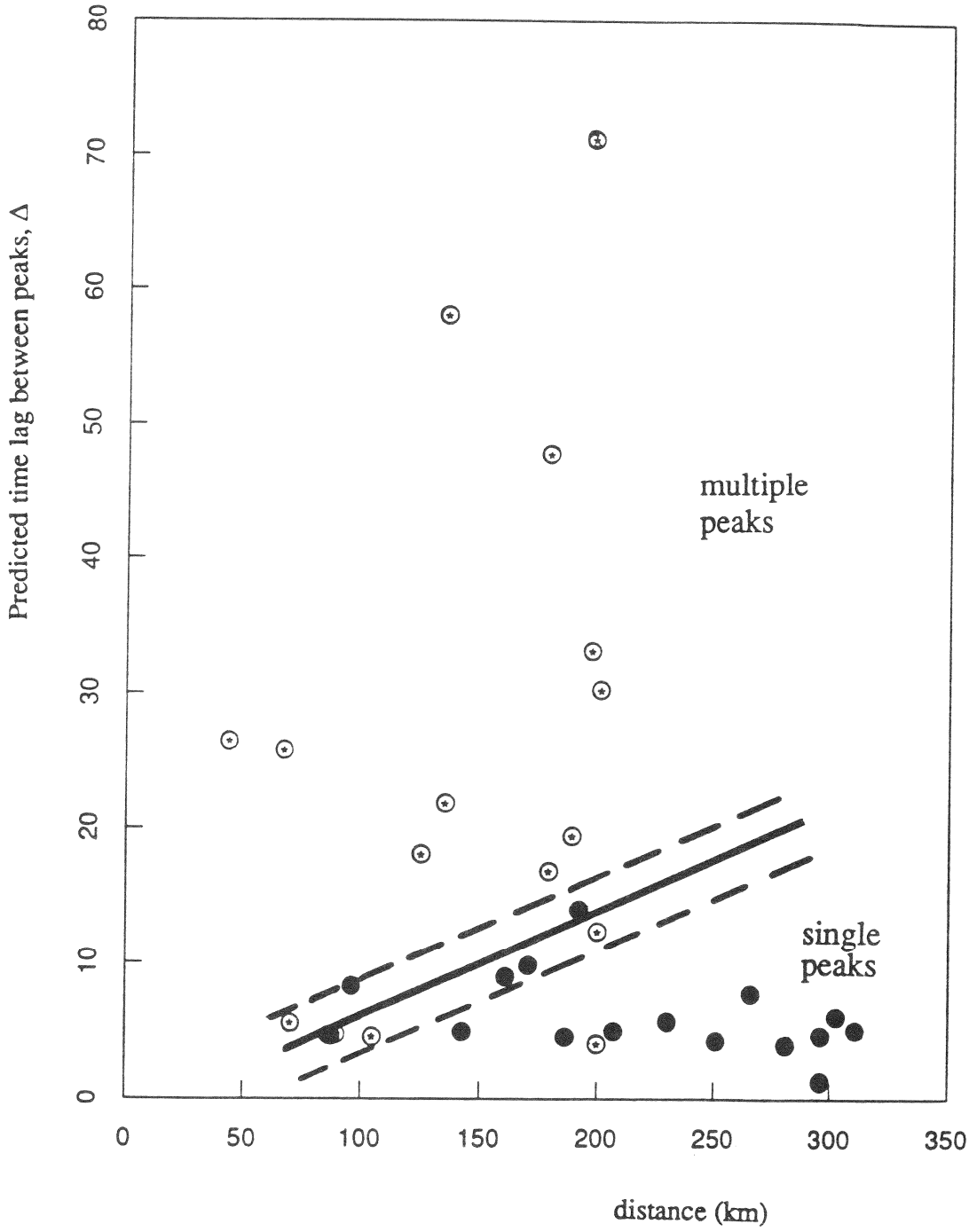

Fig. 4.5 Prediction of Multiple Peaks (open circles indicate multiple periods of shaking and closed circles indicate single period of shaking).

SECTION 5
CONCLUSIONS

Currently, methods for simulating ground motion for multiple event earthquakes are not available. In this report, a procedure is presented based on the ARMA modeling procedure in Ellis, et al. (1988). This procedure may be used to generate multiple realizations of a given accelerogram, or more importantly for the engineer, it can be used to simulate accelerograms for a site where no ground motion has been recorded. To simulate an accelerogram for a site, the location of nearby faults must first be identified. Also, soil conditions at the site must be measured. Thus, given the source and site variables, accelerograms can be simulated from the developed parametric relationships.

To simulate the possible range of ground motion, accelerograms can be simulated for numerous possible locations of subevents along the fault. Also, the variability of the ground motion for similar physical conditions may be studied by varying the value of the modeling parameters using the standard errors calculated in the regression analysis. From this suite of simulated accelerograms, seismic hazard curves for a given level of risk may be developed for the site.

SECTION 6
REFERENCES

(1) Aki, K. (1978). "Origin of the seismic gap: what initiates and stops a rupture propagation along a plate boundary?", *Proceedings of Conference VI: Methodology for Identifying Seismic Gaps and Soon-to-Break Gaps,* U.S. Geol. Surv. Open-File Rep., 78-943: 3-46.

(2) Anderson, J. G., P. Bodin, J. N. Brune, J. Prince, S. K. Singh, R. Quaas and M. Onate (1986). "Strong Ground Motion from the Michoacan, Mexico Earthquake," *Science,* Volume 233, 1043-1049.

(3) Box, G. E. P. and G. M. Jenkins (1976). *Time Series Analysis Forecasting and Control,* Holden-Day, San Francisco.

(4) Chang, M. K., J. W. Kwiatkowski, R. F. Nau, R. M. Oliver and K. S. Pister (1982). "ARMA Models for Earthquake Ground Motions," *Earthquake Engineering and Structural Dynamics,* Vol. 10, 651-662.

(5) Ellis, G. W., A. S. Cakmak and J. Ledolter (1987). "Modeling Earthquake Ground Motions in Seismically Active Regions Using Parametric Time Series Methods," *Third International Conference on Soil Dynamics and Earthquake Engineering,* 551-566.

(6) Ellis, G. W., R. DeVeaux and A. S. Cakmak (1988). "Multivariate Time Series Modeling of Strong Motion Accelerograms Recorded in Mexico and Taiwan," *Soil Dynamics and Earthquake Engineering,* in press.

(7) Fukao, Y. and M. Furumoto (1975). "Foreshocks and Multiple Shocks of Large Earthquakes," *Physics of the Earth and Planetary Interiors,* Vol. 10, 355-368.

(8) Gersch, W. and G. Kitagawa (1985). "A Time Varying AR Coefficient Model for Modeling and Simulating Earthquake Ground Motion," *Earthquake Engineering and Structural Dynamics,* Vol. 13, 243-254.

(9) International Mathematical and Statistical Library 1 (1977). Reference Manual, Houston, Texas.

(10) Jurkevics, A. and T. J. Ulrych (1979). "Autoregressive Parameters for a Suite of Strong Motion Accelerograms," *Bulletin of the Seismological Society of America,* Vol. 69, 2025-2036.

(11) Kanamori, H. (1971). "Focal Mechanism of the Tokachi-Oki Earthquake of May 16, 1968: Contortion of the Lithosphere at a Junction of Two Trenches," *Tectonophysics,* Vol. 12, 1-13.

(12) Kozin, F. (1977). "Estimation and Modeling of Non-stationary Time Series," *Proceedings of the Symposium on Computer Methods in Engineering,* University of Southern California.

(13) Mori, J. and K. Shimazaki (1984). "High Stress Drops of Short-Period Subevents from the 1968 Tokachi-Oki Earthquake as Observed on Strong-Motion Records," *Bulletin of the Seismological Society of America,* Vol. 74, 1529-1544.

(14) Polhemus, N. W. and A. S. Cakmak (1981). "Simulation of Earthquake Ground Motions Using Autoregressive Moving Average (ARMA) Models," *Earthquake Engineering and Structural Dynamics,* Vol. 9, 343-354.

(15) Port and Harbour Research Institute (1968). "Strong-Motion Earthquake Records on the 1968 Tokachi-Oki Earthquake and Its Aftershocks," Technical Note of the Port and Harbour Research Institute, Japan, No. 80.

(16) Port and Harbour Research Institute (1979). "Strong-Motion Earthquake Records on the 1978 Miyagi-Ken-Oki Earthquake in Port Area," Technical Note of the Port and Harbour Research Institute, Japan, No. 319.

(17) Port and Harbour Research Institute (1983). "Strong-Motion Earthquake Records on the 1983 Nipponkai-Chubu Earthquake in Port Area," Technical Note of the Port and Harbour Research Institute, Japan.

(18) Public Works Research Institute. "Strong Motion Earthquake Accelerograms observed on Structures," No. 1-4. Technical Note of the Public Works Research Institute, Japan.

(19) Sato, T. (1985). "Rupture Characteristics of the 1983 Nihonkai-Chubu (Japan Sea) Earthquake as Inferred from Strong Motion Accelerograms," *J. Phys. Earth,* Vol. 33, 525-557.

(20) Sawada, Y., S. Sasaki, H. Yajima and K. Ishida. "Study for the Characteristic of Seismic Design Spectra, (1) Properties of Accelerograms on Rock," Technical Report of the Central Research Institute of Electric Power Industry No. 385045, 1-41.

(21) Seno, T., K. Shimazaki, P. Somerville, K. Sudo, and T. Eguchi, (1980). "Rupture Process of the Miyagi-Oki, Japan, Earthquake of June 12, 1978," *Physics of the Earth and Planetary Interiors,* Vol. 23, 39-61.

NATIONAL CENTER FOR EARTHQUAKE ENGINEERING RESEARCH
LIST OF PUBLISHED TECHNICAL REPORTS

The National Center for Earthquake Engineering Research (NCEER) publishes technical reports on a variety of subjects related to earthquake engineering written by authors funded through NCEER. These reports are available from both NCEER's Publications Department and the National Technical Information Service (NTIS). Requests for reports should be directed to the Publications Department, National Center for Earthquake Engineering Research, State University of New York at Buffalo, Red Jacket Quadrangle, Buffalo, New York 14261. Reports can also be requested through NTIS, 5285 Port Royal Road, Springfield, Virginia 22161. NTIS accession numbers are shown in parenthesis, if available.

NCEER-87-0001 "First-Year Program in Research, Education and Technology Transfer," 3/5/87, (PB88-134275/AS).

NCEER-87-0002 "Experimental Evaluation of Instantaneous Optimal Algorithms for Structural Control," by R.C. Lin, T.T. Soong and A.M. Reinhorn, 4/20/87, (PB88-134341/AS).

NCEER-87-0003 "Experimentation Using the Earthquake Simulation Facilities at University at Buffalo," by A.M. Reinhorn and R.L. Ketter, to be published.

NCEER-87-0004 "The System Characteristics and Performance of a Shaking Table," by J.S. Hwang, K.C. Chang and G.C. Lee, 6/1/87, (PB88-134259/AS).

NCEER-87-0005 "A Finite Element Formulation for Nonlinear Viscoplastic Material Using a Q Model," by O. Gyebi and G. Dasgupta, 11/2/87, (PB88-213764/AS).

NCEER-87-0006 "Symbolic Manipulation Program (SMP) - Algebraic Codes for Two and Three Dimensional Finite Element Formulations," by X. Lee and G. Dasgupta, 11/9/87, (PB88-219522/AS).

NCEER-87-0007 "Instantaneous Optimal Control Laws for Tall Buildings Under Seismic Excitations," by J.N. Yang, A. Akbarpour and P. Ghaemmaghami, 6/10/87, (PB88-134333/AS).

NCEER-87-0008 "IDARC: Inelastic Damage Analysis of Reinforced Concrete Frame - Shear-Wall Structures," by Y.J. Park, A.M. Reinhorn and S.K. Kunnath, 7/20/87, (PB88-134325/AS).

NCEER-87-0009 "Liquefaction Potential for New York State: A Preliminary Report on Sites in Manhattan and Buffalo," by M. Budhu, V. Vijayakumar, R.F. Giese and L. Baumgras, 8/31/87, (PB88-163704/AS). This report is available only through NTIS (see address given above).

NCEER-87-0010 "Vertical and Torsional Vibration of Foundations in Inhomogeneous Media," by A.S. Veletsos and K.W. Dotson, 6/1/87, (PB88-134291/AS).

NCEER-87-0011 "Seismic Probabilistic Risk Assessment and Seismic Margins Studies for Nuclear Power Plants," by Howard H.M. Hwang, 6/15/87, (PB88-134267/AS). This report is available only through NTIS (see address given above).

NCEER-87-0012 "Parametric Studies of Frequency Response of Secondary Systems Under Ground-Acceleration Excitations," by Y. Yong and Y.K. Lin, 6/10/87, (PB88-134309/AS).

NCEER-87-0013 "Frequency Response of Secondary Systems Under Seismic Excitation," by J.A. HoLung, J. Cai and Y.K. Lin, 7/31/87, (PB88-134317/AS).

NCEER-87-0014 "Modelling Earthquake Ground Motions in Seismically Active Regions Using Parametric Time Series Methods," by G.W. Ellis and A.S. Cakmak, 8/25/87, (PB88-134283/AS).

NCEER-87-0015 "Detection and Assessment of Seismic Structural Damage," by E. DiPasquale and A.S. Cakmak, 8/25/87, (PB88-163712/AS).

NCEER-87-0016 "Pipeline Experiment at Parkfield, California," by J. Isenberg and E. Richardson, 9/15/87, (PB88-163720/AS).

NCEER-87-0017 "Digital Simulation of Seismic Ground Motion," by M. Shinozuka, G. Deodatis and T. Harada, 8/31/87, (PB88-155197/AS). This report is available only through NTIS (see address given above).

NCEER-87-0018 "Practical Considerations for Structural Control: System Uncertainty, System Time Delay and Truncation of Small Control Forces," J.N. Yang and A. Akbarpour, 8/10/87, (PB88-163738/AS).

NCEER-87-0019 "Modal Analysis of Nonclassically Damped Structural Systems Using Canonical Transformation," by J.N. Yang, S. Sarkani and F.X. Long, 9/27/87, (PB88-187851/AS).

NCEER-87-0020 "A Nonstationary Solution in Random Vibration Theory," by J.R. Red-Horse and P.D. Spanos, 11/3/87, (PB88-163746/AS).

NCEER-87-0021 "Horizontal Impedances for Radially Inhomogeneous Viscoelastic Soil Layers," by A.S. Veletsos and K.W. Dotson, 10/15/87, (PB88-150859/AS).

NCEER-87-0022 "Seismic Damage Assessment of Reinforced Concrete Members," by Y.S. Chung, C. Meyer and M. Shinozuka, 10/9/87, (PB88-150867/AS). This report is available only through NTIS (see address given above).

NCEER-87-0023 "Active Structural Control in Civil Engineering," by T.T. Soong, 11/11/87, (PB88-187778/AS).

NCEER-87-0024 Vertical and Torsional Impedances for Radially Inhomogeneous Viscoelastic Soil Layers," by K.W. Dotson and A.S. Veletsos, 12/87, (PB88-187786/AS).

NCEER-87-0025 "Proceedings from the Symposium on Seismic Hazards, Ground Motions, Soil-Liquefaction and Engineering Practice in Eastern North America," October 20-22, 1987, edited by K.H. Jacob, 12/87, (PB88-188115/AS).

NCEER-87-0026 "Report on the Whittier-Narrows, California, Earthquake of October 1, 1987," by J. Pantelic and A. Reinhorn, 11/87, (PB88-187752/AS). This report is available only through NTIS (see address given above).

NCEER-87-0027 "Design of a Modular Program for Transient Nonlinear Analysis of Large 3-D Building Structures," by S. Srivastav and J.F. Abel, 12/30/87, (PB88-187950/AS).

NCEER-87-0028 "Second-Year Program in Research, Education and Technology Transfer," 3/8/88, (PB88-219480/AS).

NCEER-88-0001 "Workshop on Seismic Computer Analysis and Design of Buildings With Interactive Graphics," by W. McGuire, J.F. Abel and C.H. Conley, 1/18/88, (PB88-187760/AS).

NCEER-88-0002 "Optimal Control of Nonlinear Flexible Structures," by J.N. Yang, F.X. Long and D. Wong, 1/22/88, (PB88-213772/AS).

NCEER-88-0003 "Substructuring Techniques in the Time Domain for Primary-Secondary Structural Systems," by G.D. Manolis and G. Juhn, 2/10/88, (PB88-213780/AS).

NCEER-88-0004 "Iterative Seismic Analysis of Primary-Secondary Systems," by A. Singhal, L.D. Lutes and P.D. Spanos, 2/23/88, (PB88-213798/AS).

NCEER-88-0005 "Stochastic Finite Element Expansion for Random Media," by P.D. Spanos and R. Ghanem, 3/14/88, (PB88-213806/AS).

NCEER-88-0006 "Combining Structural Optimization and Structural Control," by F.Y. Cheng and C.P. Pantelides, 1/10/88, (PB88-213814/AS).

NCEER-88-0007 "Seismic Performance Assessment of Code-Designed Structures," by H.H-M. Hwang, J-W. Jaw and H-J. Shau, 3/20/88, (PB88-219423/AS).

NCEER-88-0008 "Reliability Analysis of Code-Designed Structures Under Natural Hazards," by H.H-M. Hwang, H. Ushiba and M. Shinozuka, 2/29/88, (PB88-229471/AS).

NCEER-88-0009 "Seismic Fragility Analysis of Shear Wall Structures," by J-W Jaw and H.H-M. Hwang, 4/30/88.

NCEER-88-0010 "Base Isolation of a Multi-Story Building Under a Harmonic Ground Motion - A Comparison of Performances of Various Systems," by F-G Fan, G. Ahmadi and I.G. Tadjbakhsh, 5/18/88.

NCEER-88-0011 "Seismic Floor Response Spectra for a Combined System by Green's Functions," by F.M. Lavelle, L.A. Bergman and P.D. Spanos, 5/1/88.

NCEER-88-0012 "A New Solution Technique for Randomly Excited Hysteretic Structures," by G.Q. Cai and Y.K. Lin, 5/16/88.

NCEER-88-0013 "A Study of Radiation Damping and Soil-Structure Interaction Effects in the Centrifuge," by K. Weissman, supervised by J.H. Prevost, 5/24/88.

NCEER-88-0014 "Parameter Identification and Implementation of a Kinematic Plasticity Model for Frictional Soils," by J.H. Prevost and D.V. Griffiths, to be published.

NCEER-88-0015 "Two- and Three- Dimensional Dynamic Finite Element Analyses of the Long Valley Dam," by D.V. Griffiths and J.H. Prevost, 6/17/88.

NCEER-88-0016 "Damage Assessment of Reinforced Concrete Structures in Eastern United States," by A.M. Reinhorn, M.J. Seidel, S.K. Kunnath and Y.J. Park, 6/15/88.

NCEER-88-0017 "Dynamic Compliance of Vertically Loaded Strip Foundations in Multilayered Viscoelastic Soils," by S. Ahmad and A.S.M. Israil, 6/17/88.

NCEER-88-0018 "An Experimental Study of Seismic Structural Response With Added Viscoelastic Dampers," by R.C. Lin, Z. Liang, T.T. Soong and R.H. Zhang, 6/30/88.

NCEER-88-0019 "Experimental Investigation of Primary - Secondary System Interaction," by G.D. Manolis, G. Juhn and A.M. Reinhorn, 5/27/88.

NCEER-88-0020 "A Response Spectrum Approach For Analysis of Nonclassically Damped Structures," by J.N. Yang, S. Sarkani and F.X. Long, 4/22/88.

NCEER-88-0021 "Seismic Interaction of Structures and Soils: Stochastic Approach," by A.S. Veletsos and A.M. Prasad, 7/21/88.

NCEER-88-0022 "Identification of the Serviceability Limit State and Detection of Seismic Structural Damage," by E. DiPasquale and A.S. Cakmak, 6/15/88.

NCEER-88-0023 "Multi-Hazard Risk Analysis: Case of a Simple Offshore Structure," by B.K. Bhartia and E.H. Vanmarcke, 7/21/88.

NCEER-88-0024 "Automated Seismic Design of Reinforced Concrete Buildings," by Y.S. Chung, C. Meyer and M. Shinozuka, 7/5/88.

NCEER-88-0025 "Experimental Study of Active Control of MDOF Structures Under Seismic Excitations," by L.L. Chung, R.C. Lin, T.T. Soong and A.M. Reinhorn, 7/10/88, (PB89-122600/AS).

NCEER-88-0026 "Earthquake Simulation Tests of a Low-Rise Metal Structure," by J.S. Hwang, K.C. Chang, G.C. Lee and R.L. Ketter, 8/1/88.

NCEER-88-0027 "Systems Study of Urban Response and Reconstruction Due to Catastrophic Earthquakes," by F. Kozin and H.K. Zhou, 9/22/88, to be published.

NCEER-88-0028 "Seismic Fragility Analysis of Plane Frame Structures," by H.H-M. Hwang and Y.K. Low, 7/31/88.

NCEER-88-0029 "Response Analysis of Stochastic Structures," by A. Kardara, C. Bucher and M. Shinozuka, 9/22/88.

NCEER-88-0030 "Nonnormal Accelerations Due to Yielding in a Primary Structure," by D.C.K. Chen and L.D. Lutes, 9/19/88.

NCEER-88-0031 "Design Approaches for Soil-Structure Interaction," by A.S. Veletsos, A.M. Prasad and Y. Tang, to be published.

NCEER-88-0032 "A Re-evaluation of Design Spectra for Seismic Damage Control," by C.J. Turkstra and A.G. Tallin, 11/7/88.

NCEER-88-0033 "The Behavior and Design of Noncontact Lap Splices Subjected to Repeated Inelastic Tensile Loading," by V.E. Sagan, P. Gergely and R.N. White, 12/8/88.

NCEER-88-0034 "Seismic Response of Pile Foundations," by S.M. Mamoon, P.K. Banerjee and S. Ahmad, 11/1/88.

NCEER-88-0035 "Modeling of R/C Building Structures With Flexible Floor Diaphragms (IDARC2)," by A.M. Reinhorn, S.K. Kunnath and N. Panahshahi, 9/7/88, to be published.

NCEER-88-0036 "Solution of the Dam-Reservoir Interaction Problem Using a Combination of FEM, BEM with Particular Integrals, Modal Analysis, and Substructuring," by C-S. Tsai, G.C. Lee and R.L. Ketter, 12/88, to be published.

NCEER-88-0037 "Optimal Placement of Actuators for Structural Control," by F.Y. Cheng and C.P. Pantelides, 8/15/88.

NCEER-88-0038 "Teflon Bearings in Aseismic Base Isolation: Experimental Studies and Mathematical Modeling," by A. Mokha, M.C. Constantinou and A.M. Reinhorn, 12/5/88, to be published.

NCEER-88-0039 "Seismic Behavior of Flat Slab High-Rise Buildings in the New York City Area," by P. Weidlinger and M. Ettouney, 10/15/88, to be published.

NCEER-88-0040 "Evaluation of the Earthquake Resistance of Existing Buildings in New York City," by P. Weidlinger and M. Ettouney, 10/15/88, to be published.

NCEER-88-0041 "Small-Scale Modeling Techniques for Reinforced Concrete Structures Subjected to Seismic Loads," by W. Kim, A. El-Attar and R.N. White, 11/22/88, to be published.

NCEER-88-0042 "Modeling Strong Ground Motion from Multiple Event Earthquakes," by G.W. Ellis and A.S. Cakmak, 10/15/88.

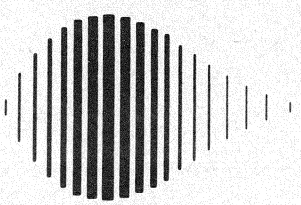

National Center for Earthquake Engineering Research
State University of New York at Buffalo